PCCP

RSC Publishing

PAPER

View Article Online
View Journal | View Issue

Excited-state dynamics of porphyrin–naphthalenediimide–porphyrin triads†

Cite this: *Phys. Chem. Chem. Phys.*, 2013, **15**, 1177

Diego Villamaina,[a] Sheshanath V. Bhosale,‡*[b] Steven J. Langford[b] and Eric Vauthey*[a]

Received 11th October 2012,
Accepted 20th November 2012

DOI: 10.1039/c2cp43595k

www.rsc.org/pccp

The excited-state dynamics of two triads consisting of a naphthalenediimide (cNDI) substituted at the core by two zinc (ZnP) or free-base tetraphenylporphyrins (FbP) was investigated by ultrafast fluorescence and transient absorption spectroscopy. The electronic absorption spectra of the triads are almost the composites of those of the constituents, pointing to a weak electronic coupling and to a localization of the excitation energy on one of the porphyrins. In cyclohexane, the excited-state dynamics of the triads are essentially the same as those of the individual porphyrins, with the exception of the Soret emission of the ZnP triad, whose lifetime exhibits a more than 10 fold shortening compared to ZnP. A similarly ultrafast fluorescence decay was measured in tetrahydrofuran and benzonitrile. In these two solvents, charge separation from the excited porphyrin to the cNDI was found to take place with ~1 ps and ~25 ps time constants in the ZnP and FbP triads, respectively. The build up of the charge-separated state population in the ZnP triad is independent of the excitation wavelength, indicating that charge separation takes place from the lowest singlet excited state. Charge recombination occurs with a time constant of around 8 ps in both triads, *i.e.* it is slower than charge separation in the ZnP triad but faster in the FbP triad. These differences are rationalized in terms of the driving forces for charge separation and recombination.

Introduction

Over the past few years, considerable efforts have been invested in the design and synthesis of complex molecular architectures aimed to mimic the functions of the photosynthetic apparatus of plants and bacteria.[1–4] In nature, solar energy is harvested by antenna complexes and funneled toward the reaction center, where it is used to achieve long-lived charge separation (CS), allowing its conversion into chemical energy. In these complex natural systems, chlorophylls play a key role in both the light collection and the CS steps and, therefore, many artificial antenna systems and reaction centers are based on porphyrins, in particular zinc and free-base tetraphenylporphyrins (ZnP and FbP), which combine broad absorption spectra in the visible region and suitable redox properties for photoinduced CS.[1,2,5–10]

ZnP constitutes one of the few exceptions of Kasha's rule, as it exhibits fluorescence from the S_2 state with a sufficient quantum yield ($\sim 8 \times 10^{-4}$)[11,12] to be detected using any standard fluorimeter.[13] This is not only due to the very large oscillator strength of the $S_2 \leftarrow S_0$ transition, responsible for the intense Soret or B band at around 420 nm, but also to the relatively slow internal conversion from this state to the lower S_1 or Q state, namely between 1 and 3 ps, depending on the solvent.[12,14,15] The latter is explained by the large S_2–S_1 energy gap and the small horizontal displacement of the S_2 and S_1 potential energy surfaces. This comparatively long lifetime allows in principle other non-radiative processes to compete with internal conversion. For example, S_2 energy hopping between ZnP units in porphyrin arrays has been observed to take place on the subpicosecond timescale.[8,16]

Photoinduced CS from the S_2 state offers the possibility to store about 1 eV more energy than CS from the S_1 state. Such CS from the local S_2 state of ZnP has been reported for several porphyrin–acceptor dyads.[17–20] For example, Mataga and co-workers, using a series of directly linked zinc porphyrin–imide dyads, have made the first observation of the Marcus inverted region for intramolecular photoinduced CS reaction.[18] Wasielewski and co-workers have shown that photoinduced

[a] *Department of Physical Chemistry, University of Geneva, 30 quai Ernest-Ansermet, CH-1211 Genève 4, Switzerland. E-mail: eric.vauthey@unige.ch*
[b] *School of Chemistry, Monash University, Clayton, Victoria 3800, Australia*

† Electronic supplementary information (ESI) available: Synthesis of the triads, additional transient absorption spectra, and calculations of the excitation energy hopping rate constants. See DOI: 10.1039/c2cp43595k

‡ Present address: School of Applied Sciences, RMIT University, GPO Box 2476V, Melbourne, Victoria 3001, Australia. E-mail: sheshanath.bhosale@rmit.edu.au

electron transfer from the S_2 state of ZnP can occur even if the donor and acceptor units are not directly linked, but covalently connected through a phenyl ring.[19] They have also found that the decay of the local S_2 state through CS is faster when the acceptor is linked to the ZnP ring at beta than at the meta position. Hammarström and co-workers have also observed CS between the S_2 state of ZnP and methylviologen in a donor–acceptor complex.[21] Our group has reported on the bimolecular quenching of ZnP in the S_2 state by both electron donors and acceptors.[22] In this case, the driving force for CS was such that the charge-separated state (CSS) was located between the S_2 and S_1 states of the ZnP unit and, as a consequence, charge recombination (CR) was found to populate the neutral ZnP in the S_1 state. Such ultrafast CR to the local S_1 state of ZnP has also been observed in a non-symmetric acceptor–ZnP–acceptor triad.[20] In most of the above cases, the CS rate constants were determined by comparing the S_2 lifetime of ZnP alone and in the dyad or upon addition of electron donor/acceptor.

The S_1 state of ZnP consists of two degenerate levels, which are split in FbP because of its lower symmetry. This results in a lower energy gap between the S_2 state and the S_1 state manifold, an acceleration of the $S_2 \rightarrow S_1$ internal conversion and a vanishingly small S_2 fluorescence quantum yield. Therefore, all the relevant photoinduced processes in FbP occur from its long-lived S_1 state.

We report here on an investigation of two triads consisting of a naphthalenediimide core substituted at 2 and 6 positions with two ZnP or FbP units (Scheme 1). Over the past few years, core-substituted naphthalenediimides (cNDIs) have regained interest because of their redox and photophysical properties.[23,24] Indeed, in contrast to NDIs substituted at the imide nitrogen atoms, that have been often used in electron donor–acceptor (D–A) systems,[4,25–27] cNDIs substituted with electron-donating groups absorb in the visible region and are generally highly fluorescent.[28] The S_1 state of these cNDIs is characterized by a substantial charge transfer character and its energy relative to the ground state decreases with the electron donating ability of the substituents, allowing the whole visible region of the spectrum to be covered upon variation of a few atoms only. The decrease in the S_1–S_0 energy gap with increasingly donating core substituents is accompanied by a parallel increase in the energies of the frontier molecular orbitals and thus by a continuous variation of the redox potentials. This makes cNDIs excellent building blocks for realizing multichromophoric systems combining light harvesting, charge separation, charge transport and redox cascades.[29–35]

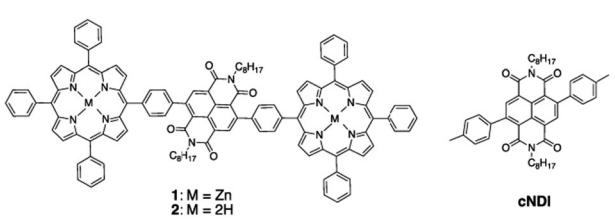

Scheme 1

Additionally, the covalent binding of electron donor units to the naphthalene core to build a D–A–D triad has been shown to increase the CS rate constant by three orders of magnitude compared to the conventional linkage *via* the imide N atoms.[36] We have recently reported on the charge transfer dynamics in two dyads consisting of a ZnP or a FbP unit linked through a rigid diaza bridge to the core of a cNDI (Scheme S1, ESI†).[37] Such binding resulted in a strong coupling between both porphyrin and cNDI units. As a consequence, the electronic absorption spectra of these dyads differed substantially from the sum of those of the individual units and the electronic excitation was delocalized over the whole dyads. Upon optical excitation, CS from the cNDI to the porphyrin unit was found to take place within 1–3 ps in medium polarity solvents. However, the large electronic coupling prevented long-lived CS, and CR time constants of 10–20 ps were measured.

The triads investigated here differ, first by the number of porphyrins, but more importantly by the linkage between the porphyrin and the cNDI units. The conformational flexibility introduced in these triads by the single bond should lead to a substantially smaller electronic coupling. Consequently, electronic excitation should remain localized on either the porphyrin or the cNDI, allowing the occurrence of CS from the S_2 state of the ZnP moiety to be envisaged. Additionally, both CS and CR can be expected to be substantially slower. We will show that although the coupling is small enough for the constituents to keep their identity, it is still large enough to result in ultrafast CS and CR. Additionally, we will show that the shortening of the S_2 lifetime of the ZnP unit in the triad compared to ZnP alone is not due to the occurrence of CS but to a perturbation of the electronic structure ZnP upon binding to cNDI.

Experimental details

Samples

The solvents cyclohexane (CHX), tetrahydrofuran (THF), and benzonitrile (BCN) were of the highest commercially available purity and were used as received. The synthesis of the triads **1** and **2** is described in detail in the ESI.† In brief, **2** was synthesized following standard Suzuki cross-coupling reaction between dibromo-NDI and monoboronic ester porphyrin in 76% yield in the presence of $Pd(PPh_3)_4$ and Na_2CO_3 in toluene.[38] The triad **1** was prepared by reacting **2** with excess $Zn(OAc)_2{\cdot}2H_2O$ in chloroform/methanol (10 : 1, v/v).

Spectroscopic measurements

Absorption spectra were recorded on a Cary 50 spectrophotometer, whereas fluorescence and excitation spectra were measured on a Cary Eclipse fluorimeter. All fluorescence spectra were corrected for the wavelength-dependent sensitivity of the detection. For fluorescence measurements, the adsorbance at the excitation wavelength was around 0.1 over 1 cm. The fluorescence quantum yields were measured using ZnP and FbP as standards.[39,40]

Fluorescence decay measurements on the nanosecond timescale were performed using the time-correlated single photon

counting (TCSPC) setup described in ref. 41 and 42. Excitation was carried out at 395 nm using a laser diode (Picoquant Model LDH-P-C-400B) generating ~60 ps pulses at 10 MHz. The full width at half maximum (FWHM) of the instrument response function (IRF) was around 200 ps.

Fluorescence dynamics occurring on a shorter timescale were measured using the fluorescence up-conversion setup described before.[22,43] Excitation was performed at 400 nm with the frequency-doubled output of a Kerr lens mode-locked Ti:sapphire laser (Mai Tai, Spectra Physics). The polarization of the pump pulses was at magic angle relative to that of the gate pulse at 800 nm. The pump intensity on the sample was of the order of 5 μJ cm^{-2}, and the FWHM of the IRF was *ca.* 200 fs. The sample solutions were located in a 0.4 mm rotating cell and had an absorbance of about 0.1 at 400 nm.

The experimental setup for the transient absorption (TA) measurements has been described in detail earlier in ref. 32 and 44. Excitation was performed at 400 nm with the frequency-doubled output of a standard 1 kHz amplified Ti:sapphire system (Spectra Physics) and at 555 nm with a home-built two-stage non-collinear optical parametric amplifier. The pump intensity on the sample was *ca.* 1–2 mJ cm^{-2}. The polarization of the probe pulses was at magic angle relative to that of the pump pulses. All spectra were corrected for the chirp of the white-light probe pulses. The FWHM of the IRF was *ca.* 150 fs. The sample solutions were placed in a 1 mm thick quartz cell and were continuously stirred by N_2 bubbling. Their absorbance at the excitation wavelength was between 0.1 and 0.2.

Computational methods

Ground-state gas-phase geometry optimization was performed at the density functional level of theory (DFT) using the B3LYP functional[45] and a [3s2p1d] basis set.[46] Electronic transitions were computed with time-dependent DFT (TD-DFT) using the same functional and basis set.[47] The calculations were carried out using Turbomole version 6.1.[48]

Results

Steady-state spectroscopy

The absorption spectra of the triads together with those of their constituting units in CHX are shown in Fig. 1. The triad spectra consist of an intense band at 417 and 416 nm for **1** and **2**, respectively, and a series of weaker bands in the 500–650 nm region. These spectra are very similar to those of the porphyrin units, with the B band at 416 and 415 nm for ZnP and FbP, respectively, and the Q bands at 545 and 583 nm for ZnP and at 512, 546, 591 and 649 nm for FbP. The cNDI unit exhibits a broad absorption band centered at around 430 nm, which is associated with the core substitution, and a structured band in the 350–390 nm region localized on the NDI center. The contribution of the cNDI to the absorption spectra of the triads can be seen as a broadening of the red edge of the B band and as a small structured band on the blue side of the B band.

The fact that the absorption spectra of the triads are essentially the composites of those of the constituents points

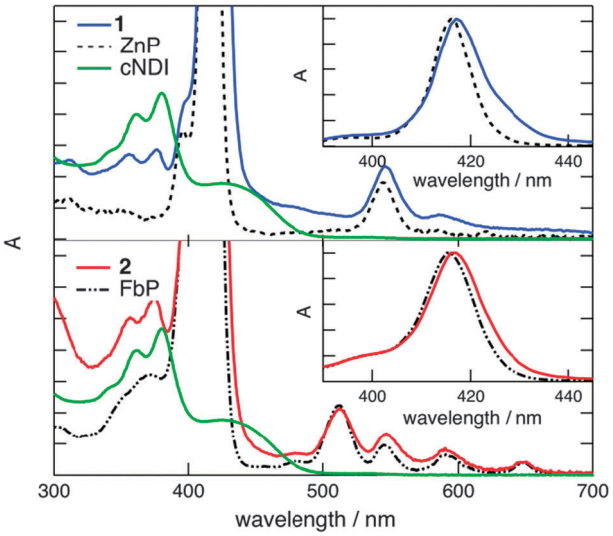

Fig. 1 Absorption spectra of the triads **1** and **2** and of the individual constituents in CHX (the insets show the B band region).

to a small electronic coupling between the chromophores and indicates that, upon photoexcitation of the triads, the electronic excitation is essentially localized on either a porphyrin unit or on the cNDI. As a consequence, the excited states of the triads directly populated upon excitation in the Q and B band of a porphyrin unit will be thereafter called local B and Q states (L_BS, L_QS), respectively, whereas the state populated upon cNDI excitation will be designed as L_NS, independently of whether the 430 nm or the ~375 nm transitions has been excited.

The probability to excite a porphyrin or the cNDI moiety of the triads at 400 nm can be estimated from the molar decadic absorption coefficient of the individual units. At 400 nm, the absorption coefficient of cNDI amounts to 6200 M^{-1} cm^{-1}, whereas those of ZnP and FbP are 40 000 and 77 400 M^{-1} cm^{-1}, respectively.[49] Thus, the relative contribution of the cNDI to the absorbance of the triads at 400 nm is only 8% and 4% for **1** and **2**, respectively. As a consequence, direct population of L_NS upon 400 nm excitation will be thereafter considered as negligible.

The emission spectra of the triads have been recorded upon $L_BS \leftarrow S_0$ and $L_QS \leftarrow S_0$ excitation in solvents of varying polarity, namely CHX, THF and BCN. Emission of **1** could only be observed in CHX and its spectrum consists of a broad band centered at around 640 nm with a shoulder on both sides (Fig. 2). By comparison, the emission spectrum of ZnP exhibits three bands, with the most intense centered at ~640 nm as well, that of medium intensity at 595 nm and the weakest one at around 700 nm. Therefore, the shoulders in the spectrum of **1** seem to coincide with the smaller emission bands of ZnP. Emission from **1** can thus be assigned to the $L_QS \rightarrow S_0$ transition. Whereas the emission spectrum of ZnP contains a distinct $S_2 \rightarrow S_0$ band at 430 nm, no $L_BS \rightarrow S_0$ emission could be detected with **1**.

Emission of **2** could be observed in all three solvents, although with different intensity. The spectrum is essentially the same as that of FbP, which consists of two bands at 654 and 719 nm (Fig. 2), and originates from the L_QS.

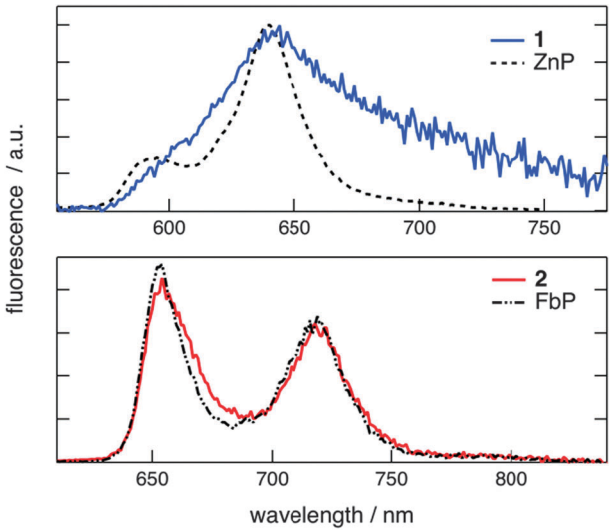

Fig. 2 Fluorescence spectra of the triads and the porphyrin constituents in CHX.

The cNDI does not exhibit any stationary fluorescence. As a consequence, the absence of any feature other than those of the porphyrins in the fluorescence spectrum of the triads does not imply that the L_NS is never populated, for example *via* excitation energy transfer (EET) from the porphyrin L_BS.

The fluorescence quantum yield of **1** and **2** determined relatively to ZnP and FbP, respectively,[12,40] depends strongly on the solvent polarity as illustrated in Table 1. The quantum yield of both triads in CHX is more than 70% that of the ZnP and FbP constituents, whereas in THF and BCN, it decreases down to ~3% for **2** and below the detection limit for **1**. Such a difference points to the opening of a new non-radiative deactivation pathway in polar solvents, most probably CS.

The absence of L_BS fluorescence with **1** can be due to an acceleration of the internal conversion to L_QS and/or to the presence of a new non-radiative pathway, namely CS or EET, to the cNDI center. In principle, the origin of this absence could be determined by comparing the L_QS fluorescence quantum yield upon L_BS and L_QS excitation. This was only possible in CHX, where **1** fluoresces. A decrease in L_QS fluorescence quantum yield of less than 10% was found on going from L_QS (544 nm) to L_BS (400 nm) excitation (Table 1), indicating that internal conversion to L_QS is the main deactivation pathway of the L_BS, at least in CHX.

Table 1 Fluorescence quantum yields of the triads, Φ_f, in different solvents relative to ZnP and FbP, measured upon 400 nm (L_BS) or 544 nm (L_QS) excitation, and fluorescence lifetimes measured by TCSPC (in CHX) or up-conversion (in THF and BCN)

Triad	Solvent	Φ_f (L_BS)	Φ_f (L_QS)	τ_f (L_BS) (ps)	τ_f (L_QS) (ps)
1	CHX	0.85	0.93	0.13	1300
1	THF	—	—	0.23	1.0
1	BCN	—	—	0.22	0.9
2	CHX	0.73			9200
2	THF	0.03			28
2	BCN	0.02			24

Because of the extremely short B fluorescence lifetime of FbP, internal conversion to L_QS can also be considered to be the main deactivation pathway of L_BS for **2**.

Time-resolved fluorescence

The fluorescence dynamics of **1** and **2** upon $L_BS \leftarrow S_0$ excitation was measured using both TCSPC and fluorescence up-conversion. Using the latter technique, it was possible to detect L_BS fluorescence of **1** at 430 nm. It was found to be much shorter-lived than that measured with ZnP, with a decay time of around 200 fs in all three solvents *vs.* 2.2 ps for ZnP in CHX and THF and 1.5 ps in BCN (Fig. 3, Table 1). These much shorter time constants agree with the vanishingly small L_BS fluorescence quantum yield of **1**.

The L_QS fluorescence lifetime of **1** in CHX measured by TCSPC amounts to 1.3 ns and is not much smaller than that of 1.8 ns reported for ZnP.[5] In THF and BCN, the fluorescence dynamics measured at 610, 640 and 660 nm was found to be dominated by a ~1 ps decay (Fig. 4). A small residual intensity with a ~2 ns component and ~1% relative intensity,

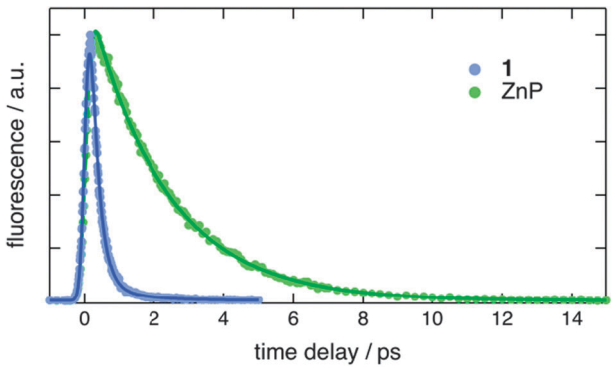

Fig. 3 L_BS fluorescence decays at 430 nm measured with triad **1** and ZnP in THF.

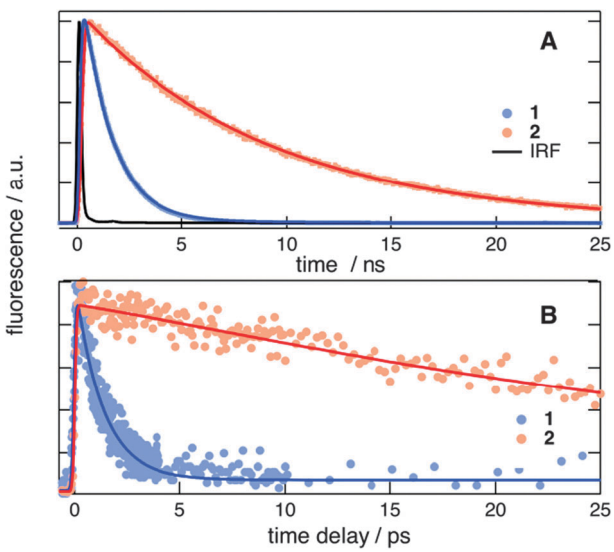

Fig. 4 L_QS fluorescence decays of the triads in CHX (A) and THF (B) upon L_BS excitation.

independent of the wavelength, was also observed. The similarity of this time constant to that found with ZnP suggests that this residual fluorescence most probably arises from some ZnP monomers present as impurity. The rise of the L_QS fluorescence from **1** upon L_BS excitation was close to the response function of the up-conversion setup, in agreement with the ultrafast decay of the L_BS fluorescence.

The L_QS fluorescence decay of **2** is also strongly solvent dependent. In CHX, it takes place on the nanosecond timescale with a time constant of 9.2 ns, whereas in THF and BCN, the fluorescence dynamics measured at several wavelengths between 640 and 710 nm is dominated by more than 90% by a decay with 28 and 24 ps time constants, respectively (Fig. 4).

Although, cNDI does not exhibit any significant stationary emission, a very short-lived fluorescence with a decay time of around 100 fs could be detected by up-conversion. Transient absorption measurements that will be discussed in a forthcoming paper point to an ultrafast decay of the emitting state to a long-lived dark state, most probably a triplet state. As will be shown below, the excited states of the cNDI unit do not play a significant role in the photophysics of the triads.

Transient absorption (TA)

The TA absorption spectra recorded with **1** in CHX (Fig. 5A) are very similar to those measured with ZnP alone (Fig. S1, ESI†). They consist of an intense negative band in the 400–430 nm region, that can be ascribed to the bleach of the $L_BS \leftarrow S_0$ transition, and of a broad positive band culminating at around 455 nm and extending to more than 700 nm with an overlapping negative feature around 545 nm that originates for the bleach of the $L_QS \leftarrow S_0$ transition. During the time window of the experiment, *i.e.* 0–2 ns, the intensity of the band decreases only partially, especially below 550 nm, and the 455 nm maximum shifts to ~470 nm. Global analysis of the time evolution of these TA spectra was performed using the sum of three exponential functions and yielded time constants of 6 ps, 1.3 ns and ≫2 ns (Fig. 5B). The same procedure, performed with the TA spectra measured with ZnP, gave time constants of 2.3 ps, 1.9 ns and ≫2 ns and the decay associated difference spectra (DADS) is displayed in Fig. S1 (ESI†). The residual TA spectra of **1** and ZnP are very similar and can thus be ascribed to the same intermediate, namely the lowest triplet state of ZnP. The 1.3 and 1.9 ns time constants are identical to the L_QS and S_1 fluorescence lifetimes of **1** and ZnP, respectively, and can thus be interpreted as the lifetime of these states decaying by fluorescence to the ground state and mainly by intersystem crossing to the triplet state. The 2.3 ps time constant obtained with ZnP can be assigned to the S_2 state lifetime, in agreement with the presence of a negative band at ~420 nm in the DADS that is due to the S_2 stimulated emission. The L_BS lifetime of **1** is too short for this state to contribute to the TA spectra. Consequently, the 6 ps time constant most probably arises from the vibrational relaxation of the hot L_QS upon internal conversion from L_BS.

Much faster changes can be observed in the TA spectra measured with **1** in THF and BCN upon $L_QS \leftarrow S_0$ excitation at 555 nm (Fig. 6). The early spectra are essentially the same as those found in CHX and assigned to L_QS absorption and

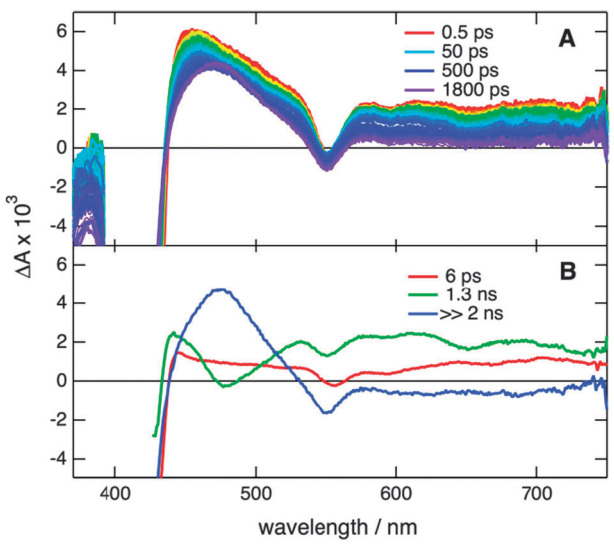

Fig. 5 (A) TA spectra recorded with **1** in CHX at different time delays after 400 nm excitation and (B) decay-associated difference spectra resulting from a global multiexponential analysis.

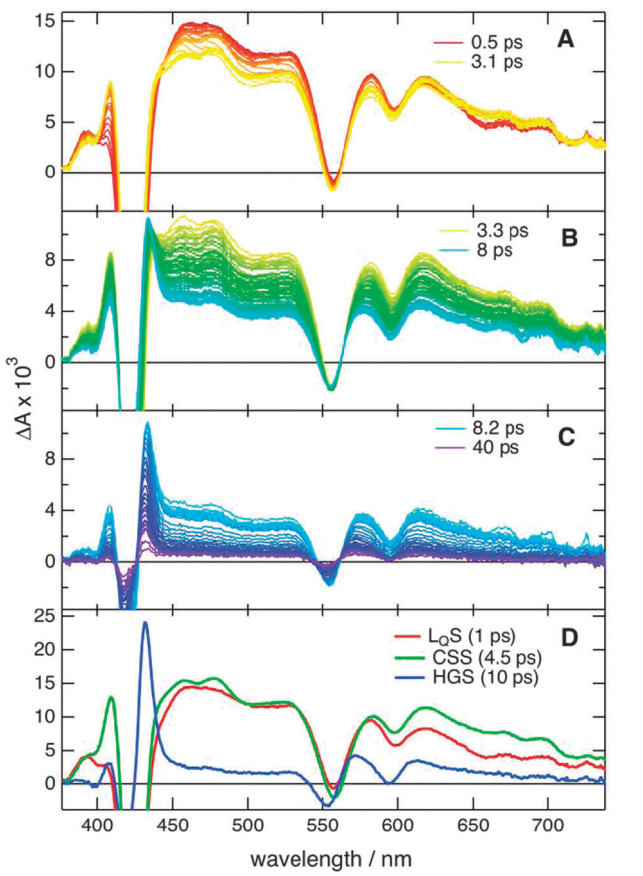

Fig. 6 (A–C) TA spectra recorded at different time delays after 555 nm excitation of triad **1** in THF and (D) species-associated difference spectra obtained from target analysis.

ground-state bleach. During the first 3 ps, the TA intensity in the 450–550 nm region decreases, whereas a parallel rise above 650 nm takes place (Fig. 6A). More importantly, a sharp band appears at 410 nm on the blue side of the $L_BS \leftarrow S_0$ bleach. During the next ~5 ps, this sharp feature as well as the TA intensity above 450 nm decrease and a new narrow band grows around 435 nm on the red side of the $L_BS \leftarrow S_0$ bleach (Fig. 6B). During the same time interval, the $L_BS \leftarrow S_0$ bleach decreases by more than 60%.

From about 8 ps onwards, the shape of the TA spectra remains essentially unchanged, but the TA intensity decreases continuously to zero within 50 ps (Fig. 6C). This strong acceleration of the excited-state dynamics of **1** on going from non-polar to polar solvents can be ascribed to the occurrence of CS from the locally-excited ZnP unit to the cNDI center. In most studies involving ZnP, occurrence of CS was observed as a rise in the TA intensity above 650 nm, as found here as well. However, a stronger support for the presence of $ZnP^{\bullet+}$ upon photoexcitation of **1** comes from the 410 nm band, which has been shown to be the most prominent feature in the electronic absorption spectrum of $ZnP^{\bullet+}$.[50] Upon photoexcitation at 400 nm instead of 555, this 410 feature is more difficult to discern, because of the scattering of the excitation light and also because the S_2 state of ZnP absorbs in this region as well (Fig. S1, ESI†). The disappearance of the $ZnP^{\bullet+}$ band observed in the 3 to ~15 ps time interval is due to the decay of the CSS population by recombination to the ground state. The band at 435 nm that grows as CR takes place can be assigned to the absorption of the vibrationally hot ground state. Indeed, if CR occurs on a timescale similar or shorter than that of vibrational cooling (VC), the instantaneous population of vibrational excited states of the electronic ground state is large enough to be observed. The hot ground state is known to be characterized by a positive TA band located on the red edge of the bleach bands.[51,52] The TA spectra recorded upon 400 nm excitation of **1** in THF are qualitatively similar to those obtained upon 555 nm excitation (Fig. S2, ESI†). The main differences are the presence of a small feature around 400–410 nm at already early time that is probably due to L_BS absorption, and a more intense hot ground state absorption band. This is in agreement with the fact that about 0.9 eV more energy is deposited into the vibrational modes of ZnP upon 400 nm than 555 nm excitation.

A global analysis of the time evolution of the TA spectra measured upon 555 nm excitation was first performed using a sum of exponential functions to determine the number of relevant time constants. In THF, one time constant was kept fixed at 1 ps to account for the decay of the L_QS as measured by fluorescence. The data could be well reproduced using three exponential functions with 1, 4.5 and 10 ps time constants. As a consequence, these data can be equally well analyzed assuming a kinetic scheme with three consecutive first order processes, with the same set of time constants.[53] Target analysis of the TA data was thus performed using the following scheme:

$$L_QS \xrightarrow{CS} CSS \xrightarrow{CR} HGS \xrightarrow{VC} GS$$

where HGS and GS stand for the hot ground state and the ground state, respectively. As expected, very good agreement with the data was obtained with the same three time constants and with the species associated difference spectra (SADS) shown in Fig. 6D. These time constants and the SADS should not be considered too literally because they have been obtained assuming that each of the three steps in the above scheme occurs from a thermally equilibrated state and follows an exponential dynamics. This is of course not true as both CS and CR occur on a similar timescale to vibrational relaxation. Therefore, non-equilibrium and, thus, non-exponential dynamics can be expected. Consequently, several processes could partially contribute to a given time constant and SADS. Despite this, the results support our assignments. Indeed, the first SADS is very similar to the TA spectra of **1** in CHX and ascribed to the L_QS, whereas the second SADS exhibits the sharp 410 nm band due to $ZnP^{\bullet+}$ and thus corresponds to the CSS. The radical anions of various cNDIs have been shown to exhibit a main absorption band centered at around 480 nm as well as some lower intensity features above 600 nm.[30,32,34] Finally, the last SADS is dominated by the intense ~430 nm band and is thus due to the hot ground state population, which relaxes to the equilibrium ground state with a 10 ps time constant. Such analysis was also performed on the TA data measured upon 400 nm excitation and yielded very similar results. Comparison of the TA time profiles at 410 and 650 nm upon 400 and 555 nm excitation shows the same rise and decay of the CSS population (Fig. 7). The initial spike in the 410 nm profile upon 400 nm excitation is most probably due to the L_BS. Global analysis of the TA data in BCN yielded time constants very similar to those in THF (Table 2).

TA measurements with **2** were performed in CHX, THF and BCN upon 400 nm excitation only. In CHX, the TA spectra are very similar to those measured with FbP alone, and consist of an intense negative band at 420 nm, due to the bleach of the $L_BS \leftarrow S_0$ transition, and a broad positive band going from

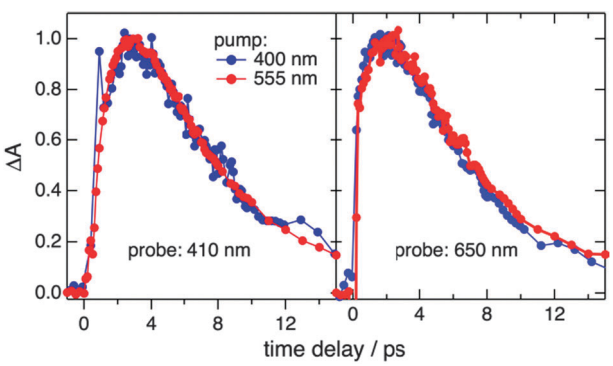

Fig. 7 Time profiles of the TA intensity at 410 and 650 nm reflecting the CSS population measured upon L_BS (400 nm) and L_QS (555 nm) excitation.

Table 2 Time constants determined from the global analysis of the TA data

Triad	Solvent	τ_{CS} (ps)	τ_{CR} (ps)	τ_{VC} (ps)
1	THF	1.0	5	10
1	BCN	0.9	8	11
2	THF	28	10	
2	BCN	24	5	

440 to more than 700 nm, due to L_QS absorption, with overlapping holes at 520, 555, 600 and 650 nm arising from the bleach of the $L_QS \leftarrow S_0$ transitions. Apart from minor variations during the first 10 ps after excitation, due most probably to vibrational relaxation of L_QS, the TA spectra remain essentially unchanged within the time window of the experiment, in agreement with the 9.2 ns fluorescence lifetime.

Like for **1**, the excited-state dynamics of **2** is substantially accelerated when going to polar solvents as shown in Fig. 8A and B. The early TA spectra are essentially the same as in CHX and can be ascribed to the L_QS population and the ground-state depletion. During the first 7 ps after excitation, a small increase in the TA intensity in the 450–500 nm region and above ~600 nm can be observed. Afterwards, the shape of the TA spectrum remains the same but the intensity decreases continuously on a ~100 ps timescale. A residual TA spectrum can still be observed at the longest time delay. From its intensity and shape, it most probably arises from free FbP present in traces. The radical cation $FbP^{\bullet+}$ has been shown to have a broad absorption band between 430 nm and 700 nm with an absorption maximum centered at 436 nm.[54–56] Thus, the observed increase in TA intensity is most probably due to the population of the CSS. The time evolution of the TA intensity at 436 nm, where $FbP^{\bullet+}$ absorbs most can be reproduced using a biexponential function with a rise time of 10 and 5 ps and a decay time of 28 and 24 ps in THF and BCN, respectively. Both decay times are identical to the fluorescence lifetimes of **1** measured in these two solvents. The fact that the observed decay time of the CSS band coincides with the L_QS fluorescence lifetime is typical of an inverted kinetics, *i.e.* a kinetics where the formation of the intermediate is slower than its decay.[57] In such case, the measured rise time corresponds to the actual decay time of the intermediate, whereas the measured decay time corresponds to the actual time constant of formation of the intermediate. To verify whether the CSS population of **2** is indeed governed by such inverted kinetics, target analysis of the TA data was performed assuming the following scheme:

$$L_QS \overset{CS}{\rightarrow} CSS \overset{CR}{\longrightarrow} GS$$

and by keeping the CS time constant fixed at 28 and 24 ps in THF and BCN, respectively. A good agreement with the TA data was obtained with CR time constants of 10 and 5 ps in THF and BCN and with the SADS shown in Fig. 8C. The first SADS is essentially identical to the TA spectra measured in CHX and is assigned to the L_QS population. The second SADS exhibits a narrower $L_BS \leftarrow S_0$ bleach, pointing to an overlapping absorption band in this region. An intense positive band with maxima at ~435 and 480 nm, and extending to more than 700 nm is also present. The narrowing of the bleach and the 435 nm maximum can be ascribed to $FbP^{\bullet+}$, whereas the 480 nm feature is most probably due to $cNDI^{\bullet-}$. On the other hand, the absorption above 550 nm could be due to both ions. The fact that the contribution of the CSS is barely visible in the TA data is in full agreement with CR faster than CS. Because of this, the CSS population does not accumulate enough to be clearly visible in the TA spectra. Due to the reduced CS time constant compared to **1**, the ground state recovery of **2** is relatively slow compared to vibrational relaxation, and, consequently, the hot ground state is not visible and does not need to be accounted for in the target analysis.

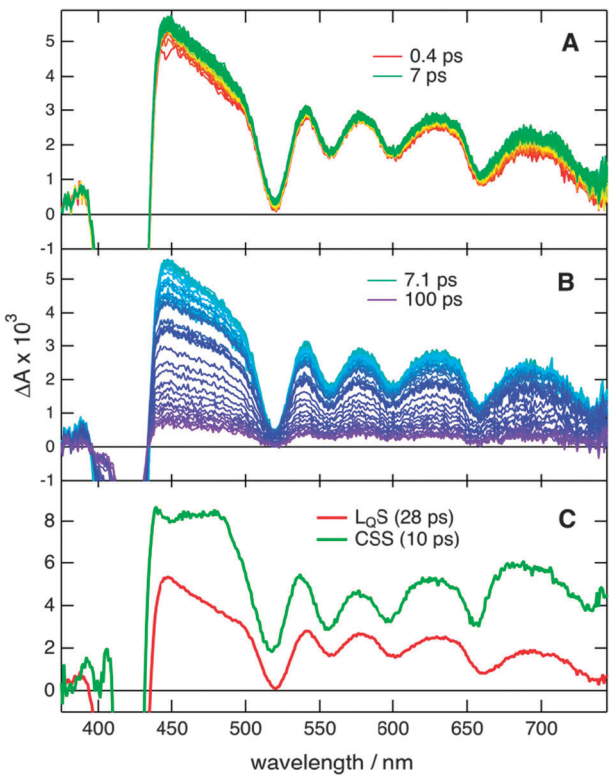

Fig. 8 (A and B) TA spectra recorded at different time delays after 400 nm excitation of triad **2** in THF and (C) species-associated difference spectra obtained from target analysis.

Discussion

The above results point rather unambiguously to the occurrence of photoinduced CS in both triads **1** and **2** in polar solvents. The existence of a low lying CS state is also supported by TD-DFT calculations that predict the lowest singlet electronic excited state to be associated with a one-electron transition from the highest occupied molecular orbital (HOMO) to the lowest unoccupied molecular orbital (LUMO) with essentially zero oscillator strength. As illustrated in Fig. 9, the HOMO is

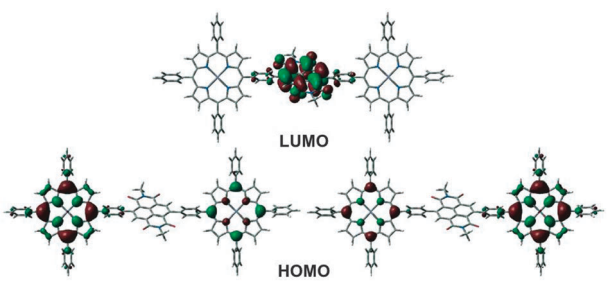

Fig. 9 Frontier molecular orbitals of triad **1** computed at the B3LYP/[3s2p1d] level of theory.

doubly degenerate with the electronic density localized almost exclusively on one ZnP, whereas the LUMO is concentrated on the central cNDI unit only. Depending on the reaction partner, porphyrins as well as cNDI can act as both electron donor and acceptor. According to both the quantum chemical calculations and the TA data, CS takes place from the excited porphyrin to the cNDI in both triads.

The CSS energy, E_{CSS}, as well as the free energy of photoinduced CS, ΔG_{CS}, have been estimated from the Weller equation:[58]

$$\Delta G_{CS} = E_{CSS} - E^* = e[E_{ox}(D) - E_{red}(A)] + C + S - E^* \quad (1)$$

where E^* is the energy of the excited state from where CS takes place, $E_{ox}(D)$ and $E_{red}(A)$ are the oxidation and reduction potential of the donor and acceptor, respectively, $C = -e^2/(4\pi\varepsilon_0\varepsilon_s d_{DA})$ is a correction term that represents the Coulombic interaction between the charged units at a distance d_{DA} and screened by a solvent of dielectric constant ε_s. Finally, S is a factor accounting for a dielectric constant of the solvent different from that used for the determination of the redox potentials, ε_s^r:

$$S = -\frac{e^2}{8\pi\varepsilon_0}\left(\frac{1}{r_D} + \frac{1}{r_A}\right)\left(\frac{1}{\varepsilon_s^r} + \frac{1}{\varepsilon_s}\right) \quad (2)$$

where r_D and r_A are the radii of the electron donating and accepting units, respectively. The values of E_{CSS} and ΔG_{CS} estimated for **1** and **2** using the excited-state energies and redox potentials measured with the individual units are listed in Table 3. Because the electron-donating and accepting units in **1** and **2** are far from spherical as assumed in the above equations, and the solvent factor S is very sensitive to the r_D and r_A values, especially in apolar solvents, the values listed in Table 3 should only be considered as indicative. Despite this, they predict rather unambiguously that, upon L_QS excitation, CS should be operative in both triads in THF and BCN, but not in CHX. This is in perfect agreement with the experimental data, *i.e.* the strong shortening of the fluorescence lifetime in THF and BCN relative to CHX and the presence of TA features in these two solvents, especially the 410 nm band due to $ZnP^{\bullet+}$, that can be ascribed to the CSS.

The energy level scheme of **1** shown in Fig. 10, together with the CS driving forces (Table 3), indicates that CS from the L_BS of

Table 3 Free energy of CS and energy of the charge-separated state calculated from eqn (1)[a]

			LE_Q		LE_B	
Triad	Solvent	E_{CSS} (eV)	E^* (eV)	ΔG_{CS} (eV)	E^* (eV)	ΔG_{CS} (eV)
1	CHX	2.3	2.1	0.2	2.95	−0.6
1	THF	1.6	2.1	−0.4	2.9	−1.3
1	BCN	1.5	2.1	−0.6	2.9	−1.4
2	CHX	2.6	1.9	0.6		
2	THF	1.9	1.9	−0.05		
2	BCN	1.7	1.9	−0.2		

[a] Using E_{ox}(ZnP) = 0.82 V, E_{ox}(FbP) = 1.08 V,[37] E_{red}(NDI) = −0.65 V,[38] r_D = 5.5 Å, r_A = 4.0 Å and d_{DA} = 11.5 Å.

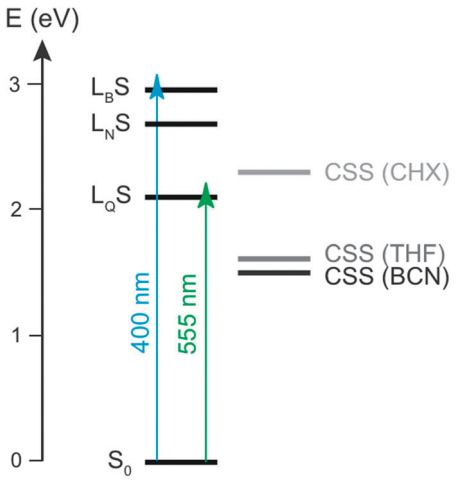

Fig. 10 Energy levels of triad **1** in various solvents.

1 is energetically favorable in all three solvents. In principle, the very short L_BS fluorescence lifetime recorded with **1**, *i.e.* between 100 and 200 fs, compared with the 2.2 ps S_2 lifetime of ZnP could be ascribed to the occurrence of CS from the upper excited state of **1**. However, this hypothesis is not supported by the other experimental data. For example, the L_QS fluorescence quantum yield of **1** is essentially the same upon 400 and 544 nm excitation (Table 1). As the CSS in CHX is above the L_QS, this could be explained by a CR to L_QS and not to the ground state, as reported previously.[20,22] However, if such sequential CS and CR were operative in CHX, the CSS should be visible in the transient spectra, in contrast to the observation. The absence of TA features due to $ZnP^{\bullet+}$ could in principle be explained by a CR much faster than CS. Assuming that the intrinsic L_BS fluorescence lifetime of **1** in the absence of CS amounts to 2.2 ps, the CS time constant would amount to ~150 fs. A CSS totally invisible by TA, even with an IRF of 200 fs, would require a CR time constant of at most 100 fs. Given that, in polar solvents, CR to the ground state takes place on the 5–10 ps timescale, such 100 fs CR to L_QS is very unlikely. Furthermore, the time evolution of the CSS population measured by TA in polar solvents is, within the limit of error, the same upon L_BS and L_QS excitation, *i.e.* exhibits a ~1 ps rise followed by a ~5 ps decay (Fig. 7). If the 200 fs L_BS fluorescence lifetime measured with **1** in polar solvents was due to CS, the time evolution of the TA signal would strongly depend on the excitation wavelength. We therefore conclude that, in this triad, CS occurs essentially from the lowest ZnP-localized excited state. The strong shortening of the L_BS lifetime of **1** compared with ZnP is most probably due to the perturbation of the ZnP electronic structure introduced by the linkage to the cNDI moiety. Such a decrease in the S_2 lifetime of ZnP upon substitution has been reported earlier.[8,15,59] Because of this, the lifetime of the L_BS is too short for CS to significantly compete with internal conversion.

The relative magnitude of the CS and CR time constants measured with **1** and **2** can be qualitatively well accounted for by the free energy associated with these processes, with $\Delta G_{CR} = -E_{CSS}$.

Indeed, the faster CS in **1** compared to **2** can be explained by the larger CS driving force and agrees with Marcus theory for electron transfer reactions occurring in the normal regime, *i.e.* a regime where the driving force is smaller than the reorganization energy.[60] Although the latter quantity for CS in these triads cannot be calculated very reliably, it can be expected to be larger than 0.6 eV in polar solvents.[61] Similarly, the slight acceleration of CS on going from THF to BCN with **2** coincides with a larger driving force in BCN, due to the better solvent stabilization of the CSS. However, this effect might be no longer operative for **1**, for which CS occurs on a similar timescale to that of solvent relaxation, the average solvation time of THF and BCN amounting to 0.94 and 5.1 ps, respectively.[62] Both solvents have relaxation components that take place on a subpicosecond timescale and, therefore, partial solvation of the CSS might be enough to ensure ultrafast electron transfer. In such a case however, the effective driving force is time dependent, and both CS and solvation dynamics are strongly entangled.[63,64]

Whereas CS is substantially faster in **1** than in **2**, CR is equally fast in both triads. This similarity is again in good agreement with the driving force for CR, which does practically not change when going from **1** to **2**. The smaller electron donating property of FbP relative to ZnP has only a weak effect on the CR dynamics. However, the CS driving force depends additionally on the energy of the excited state, E^*, which is lower for FbP than for ZnP, and is thus more favorable for ZnP than for FbP.

Excitation energy hopping (EEH) and transfer (EET) are major excited-state processes in porphyrin arrays.[8,65,66] In the triads, EEH between the porphyrin units as well as EET from ZnP in the L_BS and the cNDI unit could take place in parallel to CS. In principle, EEH could be evidenced from the measurements of the fluorescence anisotropy of the porphyrin units. However, if the two porphyrins are coplanar, as predicted by the quantum chemistry calculations, EEH does not lead to a depolarization of the fluorescence. In fact, the barrier for torsion of the porphyrins is low,[67] and thus some depolarization of the fluorescence can be expected upon EEH. The probability of EEH(T) has been estimated using Förster theory, where the EEH(T) rate constant, in ps^{-1}, can be expressed as:[68]

$$k_{EEH(T)} = 1.18\ (ps^{-1}\ cm)\cdot|V_{dd}|^2\Theta \qquad (3)$$

where V_{dd} is the interaction energy in cm^{-1} between the transition dipole of the energy donor and that of the acceptor and Θ is the spectral overlap integral, obtained from the area-normalized emission and absorption bands of the donor and acceptor, respectively, represented on a wavenumber scale. This expression was used to estimate the L_BS and L_QS EEH between the ZnP units in **1**, the EET between the ZnP unit in the L_BS and the cNDI center and finally the L_QS EEH between the FbP moieties in **2**. The resulting rate constants together with the V_{dd} values, calculated as described in the ESI,† are listed in Table 4.

Although these values should not be considered too literally, they indicate that internal conversion from L_BS of **1** is too fast for EEH to the other ZnP or EET to cNDI to be very significant in all solvents investigated. Exchange interaction is also known to favor EEH(T), especially in bridged systems.[65,69] However, as the porphyrin units are relatively far apart (~23 Å), this interaction energy should not exceed 10–20 cm^{-1}, and should thus not lead to major L_BS EEH. On the other hand, the exchange interaction between ZnP and cNDI could be expected to be larger, due to the smaller distance. Despite this, EET with a ~200 fs time constant would require an unrealistically large coupling energy of about 300 cm^{-1}. In the same way, because of the occurrence of CS, the L_QS lifetime in polar solvents is too short for EEH to take place even if exchange interaction is accounted for. However, L_QS EEH is most probably operative in CHX. The presence of two porphyrin units in these triads leads only to an increase in the absorption cross section relatively to a dyad with only one porphyrin. This additional unit should have a minor effect on the CS and CR dynamics. The situation would be different if excitation was on the NDI centre. In this case, a faster CS would be expected as the excited chromophore would be surrounded by two quenching units.

Table 4 Rate constants of Förster excitation energy hopping or transfer, $k_{EEH(T)}$, in the triads calculated from eqn (3)

Triad	Donor	Acceptor	$\lvert V_{dd}\rvert$ (cm^{-1})	Θ (cm)	$1/k_{EEH(T)}$ (ps)
1	ZnP (LE_B)	ZnP (LE_B)	47	5.7×10^{-4}	0.7
1	ZnP (LE_B)	NDI (LE_N)	35	5.4×10^{-5}	12
1	ZnP (LE_Q)	ZnP (LE_Q)	3.8	5.2×10^{-5}	1100
2	FbP (LE_Q)	FbP (LE_Q)	3.8	3.7×10^{-5}	1700

Conclusions

The electron transfer dynamics of the two triads investigated here does not differ much from that measured in ZnP–cNDI and FbP–cNDI dyads, where a rigid diaza bridge to the NDI core introduced a large coupling between the constituents that was clearly visible in the absorption spectra.[37] Charge separation was found to be only operative in polar solvents, with time constants of 1.2 and 3.6 ps for the ZnP and FbP dyads, respectively, and with charge recombination time constants of ~7 and 16 ps. Going from ZnP to FbP leads to a 3 fold slowing down of charge separation in the dyads compared to a factor of ~25 in the triads investigated here. This difference is most probably due to the large coupling that results in a partial delocalization of the excited state over the whole dyad. This leads to a partial loss of identity of the individual chromophoric units and, as a consequence, the differences between ZnP and FbP in these dyads are much less marked than in triads **1** and **2**.

On the other hand, the timescale for charge separation in the dyads and triads is similar, despite the much larger coupling in the former being most probably due to the driving force that is around zero. This comparison illustrates how a more favorable driving force can balance a smaller electronic coupling and *vice versa*.

No upper excited-state emission could be detected from the ZnP–cNDI dyad, because of the large perturbation of the

electronic structure of the ZnP unit brought about by the bridging. Ultrafast internal conversion of the upper excited state was confirmed by the finding that the charge transfer dynamics of this dyad was the same upon 400 and 625 nm excitation. In contrast, emission from the localized B state, with a lifetime ~10 times smaller than that of free ZnP, is observed with the ZnP triad. However, this shortening does not arise from the occurrence of charge separation and is most probably a consequence of the presence of the bridge as well. This result shows that the observation of a reduced upper excited-state lifetime is not sufficient for the occurrence of charge separation from this state to be concluded.

List of Abbreviations

CS, CSS	charge separation, charge-separated state
CR	charge recombination
D–A	electron donor–acceptor
D(S)ADS	decay (species) associated difference spectrum
EEH(T)	excitation energy hopping (transfer)
L_XS	locally-excited X state, X = B (porphyrin), Q (porphyrin), N (NDI)

Acknowledgements

This work was supported by the Fonds National Suisse de la Recherche Scientifique through Project Nr. 200020-124393 and the University of Geneva. S. V. Bhosale gratefully acknowledges the Australian Research Council for support under Future Fellowship through their Discovery program and RMIT University for facilities.

Notes and references

1 M. R. Wasielewski, *J. Org. Chem.*, 2006, **71**, 5051–5066.
2 D. Gust, T. A. Moore and A. L. Moore, *Acc. Chem. Res.*, 2009, **42**, 1890–1898.
3 G. Bottari, G. de la Torre, D. M. Guldi and T. s. Torres, *Chem. Rev.*, 2010, **110**, 6768–6816.
4 M. Borgström, N. Shaikh, O. Johansson, M. F. Anderlund, S. Styring, B. Aakermark, A. Magnuson and L. Hammarström, *J. Am. Chem. Soc.*, 2005, **127**, 17504–17515.
5 P. Brodard, S. Matzinger, E. Vauthey, O. Mongin, C. Papamicaël and A. Gossauer, *J. Phys. Chem. A*, 1999, **103**, 5858.
6 E. K. L. Yeow, K. P. Ghiggino, J. N. H. Reek, M. J. Crossley, A. W. Bosman, A. P. H. J. Schenning and E. W. Meijer, *J. Phys. Chem. B*, 2000, **104**, 2596–2606.
7 D. Holten, D. F. Bocian and J. S. Lindsey, *Acc. Chem. Res.*, 2002, **35**, 57.
8 A. Morandeira, E. Vauthey, A. Schuwey and A. Gossauer, *J. Phys. Chem. A*, 2004, **108**, 5741–5751.
9 N. Aratani, D. Kim and A. Osuka, *Acc. Chem. Res.*, 2009, **42**, 1922–1934.
10 M. C. O'Sullivan, J. K. Sprafke, D. V. Kondratuk, C. Rinfray, T. D. W. Claridge, A. Saywell, M. O. Blunt, J. N. O'Shea, P. H. Beton, M. Malfois and H. L. Anderson, *Nature*, 2011, **469**, 72–75.
11 D. J. Quimby and F. R. Longo, *J. Am. Chem. Soc.*, 1975, **97**, 5111–5117.
12 H.-Z. Yu, J. S. Baskin and A. H. Zewail, *J. Phys. Chem.*, 2002, **106**, 9845.
13 O. Ohno, Y. Kaizu and H. Kobayashi, *J. Chem. Phys.*, 1985, **82**, 1779–1787.
14 G. G. Gurzadyan, T.-H. Tran-Thi and T. Gustavsson, *J. Chem. Phys.*, 1998, **108**, 385–388.
15 X. Liu, U. Tripathy, S. V. Bhosale, S. J. Langford and R. P. Steer, *J. Phys. Chem. A*, 2008, **112**, 8986–8998.
16 A. Nakano, Y. Yasuda, T. Yamasaki, S. Akimoto, I. Yamazaki, H. Miyasaka, A. Itaya, M. Murakami and A. Osuka, *J. Phys. Chem. A*, 2001, **105**, 4822–4833.
17 D. LeGourriérec, M. Andersson, J. Davidsson, E. Mukhtar, L. Sun and L. Hammarström, *J. Phys. Chem. A*, 1999, **103**, 557–559.
18 N. Mataga, H. Chosrowjan, S. Taniguchi and Y. Shibata, *J. Phys. Chem.*, 2002, **106**, 12191–12201.
19 R. T. Hayes, C. J. Walsh and M. R. Wasielewski, *J. Phys. Chem. A*, 2004, **108**, 2375–2381.
20 S. Wallin, C. Monnereau, E. Blart, J.-R. Gankou, F. Odobel and L. Hammarström, *J. Phys. Chem. A*, 2010, **114**, 1709–1721.
21 M. Andersson, J. Davidsson, L. Hammarström, J. Korppi-Tommola and T. Peltola, *J. Phys. Chem. B*, 1999, **103**, 3258–3262.
22 A. Morandeira, L. Engeli and E. Vauthey, *J. Phys. Chem. A*, 2002, **106**, 4833–4837.
23 N. Sakai, J. Mareda, E. Vauthey and S. Matile, *Chem. Commun.*, 2010, **46**, 4225–4237.
24 S. V. Bhosale, S. V. Bhosale and S. K. Bhargava, *Org. Biomol. Chem.*, 2012, **10**, 6455–6468.
25 S. R. Greenfield, W. A. Svec, D. Gosztola and M. R. Wasielewski, *J. Am. Chem. Soc.*, 1996, **118**, 6767–6777.
26 K. P. Ghiggino, J. A. Hutchison, S. J. Langford, M. J. Latter, M. A. P. Lee and M. Takezaki, *Aust. J. Chem.*, 2006, **59**, 179–185.
27 I. V. Sazanovich, M. A. H. Alamiry, J. Best, R. D. Bennett, O. V. Bouganov, E. S. Davies, V. P. Grivin, A. J. H. M. Meijer, V. F. Plyusnin, K. L. Ronayne, A. H. Shelton, S. A. Tikhomirov, M. Towrie and J. A. Weinstein, *Inorg. Chem.*, 2008, **47**, 10432–10445.
28 F. Würthner, A. Shahadat, C. Thalacker and T. Debaerdemaeker, *Chem.–Eur. J.*, 2002, **8**, 4742.
29 S. Bhosale, S. A. L. P. Talukdar, A. Fürstenberg, N. Banerji, E. Vauthey, G. Bollot, J. Mareda, C. Röger, F. Würthner, N. Sakai and S. Matile, *Science*, 2006, **313**, 84–86.
30 N. Banerji, A. Fürstenberg, S. Bhosale, A. L. Sisson, N. Sakai, S. Matile and E. Vauthey, *J. Phys. Chem. B*, 2008, **112**, 8912–8922.
31 A. L. Sisson, N. Sakai, N. Banerji, A. Fürstenberg, E. Vauthey and S. Matile, *Angew. Chem., Int. Ed.*, 2008, **47**, 3727–3729.
32 N. Banerji, G. Duvanel, A. Perez-Velasco, S. Maity, N. Sakai, S. Matile and E. Vauthey, *J. Phys. Chem. A*, 2009, **113**, 8202–8212.
33 R. Bhosale, J. Misek, N. Sakai and S. Matile, *Chem. Soc. Rev.*, 2010, **39**, 138–149.
34 N. Sakai, M. Lista, O. Kel, S.-i. Sakurai, D. Emery, J. Mareda, E. Vauthey and S. Matile, *J. Am. Chem. Soc.*, 2011, **133**, 15224–15227.
35 E. Vauthey, *ChemPhysChem*, 2012, **13**, 2001–2011.
36 F. Chaignon, M. Falkenstrom, S. Karlsson, E. Blart, F. Odobel and L. Hammarström, *Chem. Commun.*, 2007, 64–66.
37 N. Banerji, S. V. Bhosale, I. Petkova, S. J. Langford and E. Vauthey, *Phys. Chem. Chem. Phys.*, 2011, **13**, 1019–1029.
38 S. V. Bhosale, M. B. Kalyankar, S. V. Bhosale, S. J. Langford, E. F. Reid and C. F. Hogan, *New J. Chem.*, 2009, **33**, 2409–2413.
39 H. Z. Liu, J. S. Baskin, B. Steiger, C. Z. Wan, F. C. Anson and A. H. Zewail, *Chem. Phys. Lett.*, 1998, **293**, 1.
40 J. S. Baskin, H.-Z. Yu and A. H. Zewail, *J. Phys. Chem.*, 2002, **106**, 9837.
41 P.-A. Muller, C. Högemann, X. Allonas, P. Jacques and E. Vauthey, *Chem. Phys. Lett.*, 2000, **326**, 321–327.
42 A. Fürstenberg, M. D. Julliard, T. G. Deligeorgiev, N. I. Gadjev, A. A. Vassilev and E. Vauthey, *J. Am. Chem. Soc.*, 2006, **128**, 7661–7669.
43 G. Duvanel, J. Grilj, H. Chaumeil, P. Jacques and E. Vauthey, *Photochem. Photobiol. Sci.*, 2010, **9**, 908–915.
44 G. Duvanel, J. Grilj, A. Schuwey, A. Gossauer and E. Vauthey, *Photochem. Photobiol. Sci.*, 2007, **6**, 956–963.
45 J. P. Perdew, *Phys. Rev. B: Condens. Matter Mater. Phys.*, 1986, **33**, 8822–8824.
46 A. Schäfer, H. Horn and R. Ahlrichs, *J. Chem. Phys.*, 1992, **97**, 2571–2577.
47 R. Bauernschmitt and R. Ahlrichs, *Chem. Phys. Lett.*, 1996, **256**, 454–464.
48 R. Ahlrichs, M. Bär and M. Häser, *Chem. Phys. Lett.*, 1989, **162**, 165–169.
49 G. D. Dorough, J. R. Miller and F. M. Huennekens, *J. Am. Chem. Soc.*, 1951, **73**, 4315–4320.

50 A. N. Okhrimenko, A. V. Gusev and M. A. J. Rodgers, *J. Phys. Chem. A*, 2005, **109**, 7653–7656.
51 J. Grilj, C. Zonca, L. M. L. Daku and E. Vauthey, *Phys. Chem. Chem. Phys.*, 2012, **14**, 6345–6351.
52 J. Grilj, P. Buchgraber and E. Vauthey, *J. Phys. Chem. A*, 2012, 7516–7522.
53 I. H. M. van Stokkum, D. S. Larsen and R. van Grondelle, *Biochim. Biophys. Acta, Bioenerg.*, 2004, **1657**, 82–104.
54 E. A. Alemán, J. Manríquez Rocha, W. Wongwitwichote, L. A. Godínez Mora-Tovar and D. A. Modarelli, *J. Phys. Chem. A*, 2011, **115**, 6456–6471.
55 Z. Gasyna, W. R. Browett and M. J. Stillman, *Inorg. Chem.*, 1985, **24**, 2440–2447.
56 C. Paliteiro and A. l. Sobral, *Electrochim. Acta*, 2005, **50**, 2445–2451.
57 C. Högemann and E. Vauthey, *J. Phys. Chem. A*, 1998, **102**, 10051–10059.
58 A. Weller, *Z. Phys.–Chem. Materialforsch.*, 1982, **133**, 93.
59 H. S. Cho, N. W. Song, Y. H. Kim, S. C. Jeoung, S. Hahn, D. Kim, S. K. Kim, N. Yoshida and A. Osuka, *J. Phys. Chem. A*, 2000, **104**, 3287.
60 R. A. Marcus and N. Sutin, *Biochim. Biophys. Acta*, 1985, **811**, 265–322.
61 N. Mataga, S. Taniguchi, H. Chosrowjan, A. Osuka and K. Kurotoby, *Chem. Phys. Lett.*, 2005, **403**, 163.
62 M. L. Horng, J. A. Gardecki, A. Papazyan and M. Maroncelli, *J. Phys. Chem.*, 1995, **99**, 17311–17337.
63 H. Sumi and R. A. Marcus, *J. Chem. Phys.*, 1986, **84**, 4814–4894.
64 O. Nicolet and E. Vauthey, *J. Phys. Chem. A*, 2002, **106**, 5553–5562.
65 K. Kilså, J. Kajanus, J. Mårtensson and B. Albinsson, *J. Phys. Chem. B*, 1999, **103**, 7329–7339.
66 N. Aratani, A. Osuka, H. S. Cho and D. Kim, *J. Photochem. Photobiol., C*, 2002, **3**, 25–52.
67 K. Petterson, A. Kyrychenko, E. Rönnow, T. Ljungdahl, J. Mårtensson and B. Albinsson, *J. Phys. Chem. A*, 2006, **110**, 310.
68 T. Pullerits, S. Hess, J. L. Herek and V. Sundström, *J. Phys. Chem. B*, 1997, **101**, 10560–10567.
69 B. Albinsson and J. Mårtensson, *J. Photochem. Photobiol., C*, 2008, **9**, 138–155.